Geometric optimization of a phase-change energy storage operating with a PV micro-installation

Optymalizacja geometrii zmiennofazowego magazynu energii współpracującego z mikroinstalacją fotowoltaiczną

DOMINIKA PORWISIAK, ZIEMOWIT MALECHA

DOI 10.36119/15.2022.7-8.3

Currently, efforts are being made to increase the share of renewable energy sources in Poland's energy mix. Energy storages, both electric and thermal, can help to overcome the disadvantages of these energy sources. A latent heat store designed to cooperate with a photovoltaic micro-installation and a cooling system was selected for testing. A numerical model of the heat storage was made and a series of numerical calculations of the charging and discharging of the heat accumulator was carried out for different geometries of the phase change medium. The processes of solidification and melting were modelled using an enthalpy-porosity approach. The obtained results were illustrated on the summary characteristics. It is shown that the shape of the phase change medium has a significant effect on the dynamics of the phase change process.
Keywords: phase-change material energy storage, computational fluid dynamics, photovoltaic micro-installation, enthalpy-porosity model

Obecnie podejmowane są działania mające na celu zwiększenie udziału odnawialnych źródeł energii w bilansie energetycznym Polski. Magazyny energii elektrycznej, jak też ciepła, mogą pomóc w przezwyciężeniu wad tych źródeł energii. Do badań wybrano magazyn ciepła utajonego przeznaczony do współpracy z mikroinstalacją fotowoltaiczną i systemem chłodzenia. Wykonano model numeryczny magazynu ciepła oraz przeprowadzono serię obliczeń numerycznych ładowania i rozładowywania akumulatora ciepła dla różnych geometrii ośrodka zmiennofazowego. Procesy krzepnięcia i topnienia modelowano z wykorzystaniem metody entalpia-porowatość. Uzyskane wyniki zilustrowano na charakterystykach zbiorczych. Wykazano, że kształt materiału zmiennofazowego ma istotny wpływ na dynamikę procesu przemiany fazowej.
Słowa kluczowe: zmiennofazowy magazyn energii, numeryczna mechanika płynów, mikroinstalacja fotowoltaiczna, model entalpia-porowatość

Introduction

The use of renewable energy sources has received a lot of attention in recent years. Due to the low stability of these sources, their use is associated with several problems. These include weather-dependent operation or high load on the electricity grid. One of the best ways to counteract these problems is to use energy storage. One of the best ways to store heat or cold is the use of latent heat storage. Many researchers are undertaking research related to combining renewable energy sources with PCM (Phase Change Material) energy storage. In [1] the solar assisted heat pump coupled with PCM heat storage system was described. In such system COP (coefficient of performance) can reach 5.79 which is 70% higher value than in conventional air conditioning systems. In [2] numerical examination of latent heat storage for concentrated solar plants was performed. According to [3] there are multiple different configurations to combine PCM with photovoltaic systems. Cui et al. in [4] states that the electrical efficiency of the PV/T system combined with PCM may increase up to 5%. Also, the thermal efficiency of such a system could be increased by around 20-30%. He also states that by applying PCM storage system, cost decreases up to 20%.

In this paper, PCM cold storage combined with PV micro-installation was considered. The geometry of PCM energy storage was analyzed and optimized to obtain the most effective geometry of the PCM medium for assumed time of charging and discharging. The current study is important because a huge amount of electrical energy obtained from photovoltaic micro – installations is fed back into the grid. This energy can be stored and the use of it can be shifted. The optimization of PCM geometry in such a system is unique and has not been studied before.

Research object

Considered PCM storage works together with photovoltaic panels and a compressor chiller. Stored cold is used for air conditioning during the night in summer months, for instance in July. People in Poland usually are away from home during the day, when the electricity production from photovoltaic cells is the highest due to the highest amount of solar radiation (Fig.1). When the householder is away, electricity consumption is reduced. In order not to transmit the electricity to the grid, the surplus energy produced feeds the compressor chiller, which charges the energy store with cold for subsequent cooling of the rooms. According to Energy Market Information Centre in Poland report [5] average power of micro photovoltaic installations in 2019 was equal to 6.5 kWp. For calculations, the installation power was assumed to be 5.6 kWp. Energy production was assumed to be 5500 kWh/year. Such micro photovoltaic installation can supply power to 2 kW compressor chiller during the time when electricity consumption is reduced and electricity power production is the highest. Assuming that the coefficient of performance of the chiller is equal to 3.5, the cold power supplied to the storage will be equal

BEng Dominika Porwisiak https://orcid.org/0000-0003-0340-2227, DSc Ziemowit Malecha https://orcid.org/0000-0001-8560-760X – Wroclaw University of Science and Technology, Department of Cryogenics and Aerospace Engineering, Wroclaw, Poland. Corresponding author: ziemowit.malecha@pwr.edu.pl

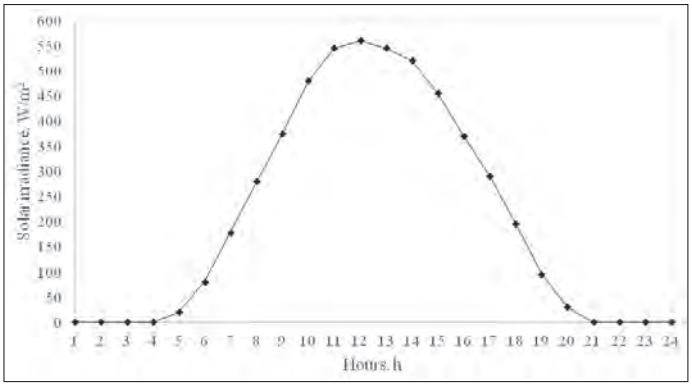

Figure 1 Distribution of average global solar irradiance for every hour in July in Warsaw [6]
Rysunek 1 Rozkład średniego natężenia promieniowania słonecznego dla każdej godziny doby w lipcu w Warszawie

to 7 kW. For this study, it has been assumed that the chiller will operate during the hours of maximum electricity production by the photovoltaic installation, from 10 a.m. to 5 p.m., which gives 7 hours of operation.

Methods

The analysis was performed using OpenFOAM software. Computational fluid dynamics governing equations are Navier-Stokes equations. These equations are based on the conservation law of the physical properties of fluid.

Mathematical model

The mathematical model applied in this study was based on the conjugate heat transfer approach. Solid and fluid regions can exchange heat through adjoining boundaries. The solidification and melting processes were modelled using the enthalpy-porosity approach.

Incompressible Navier-Stokes equations were applied to model the dynamics of the flow in the liquid region (1), where **u** is the velocity vector, ρ is the density and μ is the dynamic viscosity.

$$u\left(\nabla u + (\nabla u)^T\right) + S_b + S_d \qquad (1)$$

The temperature field was modelled by applying the energy conservation equation (2), where $h = C_p T, \lambda$ is the thermal conductivity and C_p is specific heat capacity, T is temperature.

$$\frac{\partial \rho h}{\partial t} + \nabla \cdot (\rho u h) = \nabla \cdot \left(\frac{\lambda}{C_p} \nabla h\right) - S_h \qquad (2)$$

To model changing of the phases the enthalpy-porosity model was applied. This model introduces an additional field to distinguish the phases ($\alpha = 1$ for liquids and $\alpha = 0$ for solids). It also assumes that phase change occurs at the melting temperature T_{melt}. Source term S_d in eq. (1) is the porosity effect formed based on Darcy's law [6]. It was added to maintain zero velocity in the frozen parts of the fluid region (3). An inverse permeability based on Carman-Koseny equation is defined by expression $(1 - \alpha)^2/\alpha^3$, C is the mushy zone constant [7]. $S_d = 0$, and $\alpha = 1$ in liquid parts of the domain and porosity term is not active. When phase change starts, α value approaches to zero and the porosity term starts to dominate all other terms in momentum equation and will be reduced.

$$S_d = -C \frac{(1-\alpha)^2}{\alpha^2} u \qquad (3)$$

Source term S_h models the release of latent heat during the phase change process in the equation. (2). It is defined by (4), where L_f is the latent heat released during the freezing process.

$$S_h = \rho L_f \left(\frac{\partial \alpha}{\partial t} + \nabla \cdot (u\alpha)\right) \qquad (4)$$

Source term S_b from the momentum equation (1) is related to buoyancy. It is based on Boussinesq approximation. S_b is defined by (5), where g is the gravity acceleration, β_T is the thermal expansion coefficient and T_{ref} is the reference temperature.

$$S_b = \rho g \beta_T (T - T_{ref}) \qquad (5)$$

In solid regions energy diffusion equation was applied to model heat transfer (6). In eq. (6) ρ is the density, λ is the thermal conductivity and C_p is the specific heat capacity characterizing the solid region.

$$\frac{\partial (\rho h)}{\partial t} = \nabla \cdot \left(\frac{\lambda}{C_p} \nabla h\right) \qquad (6)$$

Numerical model

For the numerical analysis one of the available solvers chtMultiRegionFoam was used. The solver includes heat transfer calculations. The simulation is transient and turbulence models are applicable. It offers the possibility to simultaneously calculate compressible fluid flow and combined heat flow in solids. It is based on the PIMPLE algorithm. OpenFoam software uses for calculations finite volume method.

For simulation, the PCM was assumed to be enclosed inside the material with a good thermal conductivity of approximately 200 W/mK (for example aluminium [8]). The dimensions of the heat storage were selected to be 1 m x 1 m x 0,85 m. The general geometry is illustrated in Fig. 2. To shorten the calculations, a two-dimensional model was adopted. The geometry consists of an inner part which is a phase-change medium and a surrounding solid body. The heat is supplied from four sides of the storage, top, bottom, right-hand side, and left-hand side. The properties of the materials defined for the simulation are shown in Table I.

Table I Thermophysical properties of the materials defined in the simulation
Tabela 1 Termofizyczne właściwości materiałów zdefiniowanych w symulacji

	PCM	Solid body
Molar mass, g/mol	240,471 [9]	26,9815
Thermal conductivity coefficient, W/mK	-	200 [10]
Heat of fusion, J/mol	-	8660 [11]
Specific heat, J/kgK	1800/2100 [12]	921 [13]
Density, kg/m³	777 [9]	2700 [14]
Dynamic viscosity coefficient, Pa·s	$4{,}21 \cdot 10^{-3}$ [15]	-
Prandtl number	7,5	-
Melting point, K	291 [12]	-
Phase change heat, J/kg	175190 [12]	-

On Figure 3 investigated geometries of PCM heat storage were illustrated. All of them have nearly the same volume of PCM material inside, which is 0,25 m³.

For every geometry a hexagonal 2D mesh was created. The mesh parameters are presented in the table. The mesh was condensed in PCM region as presented on Figure 4.

Table 2 Number of mesh elements in every case
Tabela 2 Liczba elementów siatki w każdym z badanych przypadków

Geometry	Number of elements
Base Geometry	39514
Horizontal ribs	118544
Vertical ribs	53232
Rollers	44173
Grid	249000

Results

The charging and discharging process was simulated for 7 hours for each geometry. Heat loss to the surroundings was neglected in calculations. Form factor stands for the ratio of the heat transfer

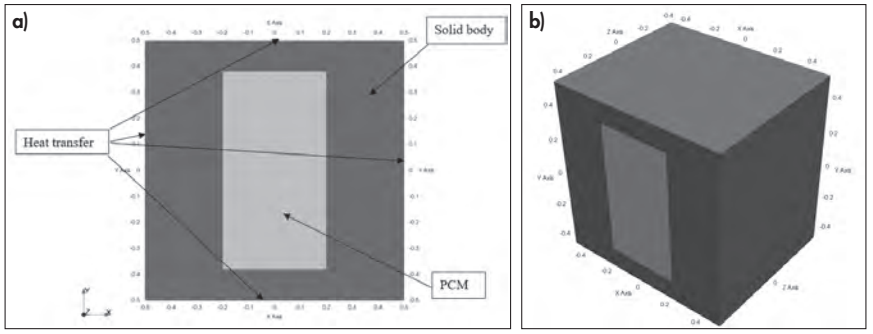

Figure 2
General geometry of PCM heat storage used in simulation. (A) front view (B) three-dimesional view
Rysunek 2 Ogólna geometria zasobnika ciepła PCM wykorzystana w symulacji: (A) widok z przodu (B) widok trójwymiarowy

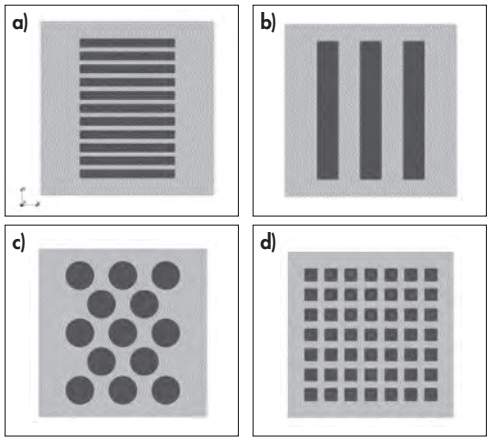

Figure 3
Geometries of PCM heat storage investigated in this study. (A) – Horizontal ribs, (B) – vertical ribs, (C) – rollers, (D) – grid
Rysunek 3 Geometrie magazynów ciepła badane w niniejszej pracy: (A) – żebra poziome, (B) – żebra pionowe, (C) – walce, (D) – krata

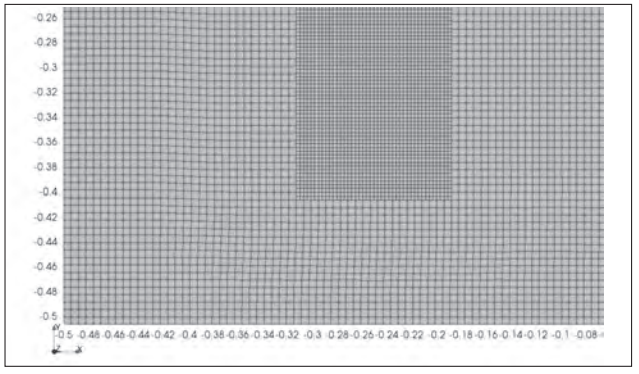

Figure 4
The detail of mesh of the geometry with vertical ribs
Rysunek 4 Widok szczegółowy siatki z pionowymi żebrami

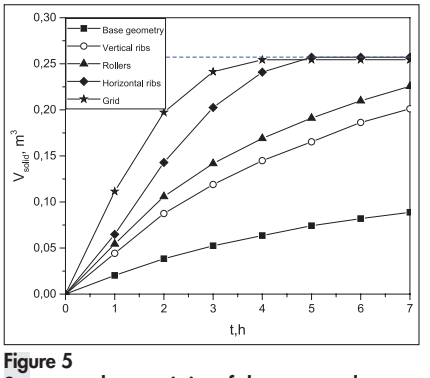

Figure 5
Summary characteristics of the measured geometries – storage charging
Rysunek 5 Charakterystyka podsumowująca badanych geometrii – ładowanie

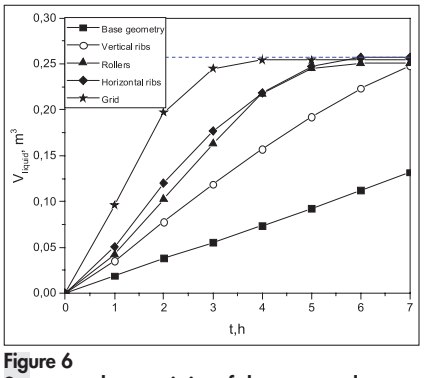

Figure 6
Summary characteristics of the measured geometries – storage discharging
Rysunek 6 Charakterystyka podsumowująca badanych geometrii – rozładowywanie

surface area between the PCM and solid material to the PCM volume. Fully charged storage should not contain any liquid phase in the PCM volume and discharged should contain only a liquid phase. As presented in Table 3. only 2 geometries fully charged and discharged (horizontal ribs and grid) during the assumed 7 hours of operation.

Based on the performed calculations, it can be concluded that the geometry of the PCM heat storage has a significant effect on the dynamics of the phase change of the working medium. In the case of storage charging, the summary results are shown in Figure 5, which illustrates the solid phase volume characteristics of the medium as a function of time. It can be unequivocally stated that the rate of phase change depends on the form factor of the geometry of the phase-change medium. The fastest process occurs for geometries with the largest form factor and the slowest process for geometries with the smallest form factor. Storage charging was fully completed for geometries with aspect ratios of 43.60 and 51.24.

Figure 6. shows similar characteristics, this time for the process of discharging the battery. In this case, the relationship between the form factor and the dynamics of the process can be observed. The discharge process was fully realized for geometries with form factor of 23.73, 43.60 and 51.24.

For the application of similar phase-change heat storage in a single-family house, the geometry of the phase-change medium would have to be adjusted such that the storage is fully charged within 7 hours and that it gives off cold (discharges) as long as possible. Of the geometries tested, this condition is best met by a geometry with horizontal ribs, with an aspect

Table 3 Compilation of results for every geometry, containing volume of PCM, form factor, volume of liquid after charging and volume of solid after discharging
Tabela 3 Porównanie wyników obliczeń dla każdej z geometrii, zawierające objętość czynnika zmiennofazowego, współczynnik kształtu, objętość fazy ciekłej po ładowaniu akumulatora oraz objętość fazy stałej po rozładowywaniu akumulatora

Geometry	Volume of PCM, m^3	Form factor	Volume of liquid PCM after 7 hours of charging, m^3	Volume of solid PCM after 7 hours of discharging, m^3
Base geometry	0.255	7.67	0.166	0.123
Horizontal ribs	0.257	46.60	0	0
Vertical ribs	0.255	18.50	0.054	0.007
Rollers	0.251	23.73	0.025	0
Grid	0.254	51.24	0	0

Table 4 Contours of phase quantity in sample geometries (From the top to bottom: base geometry, Rollers, Grid). α = 0 (blue) for solid state, 1 (red) for liquid
Tabela 4 Kontury zawartości danej fazy w przykładowych geometriach (Od góry: geometria bazowa, walce, krata). α = 0 (niebieski) dla ciała stałego, 1 dla płynu

	1 hour	4 hours	7 hours
Base geometry			
Charging	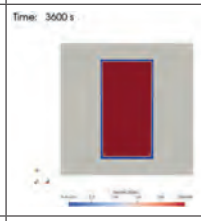	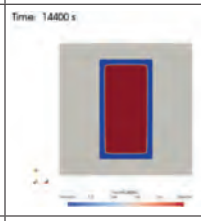	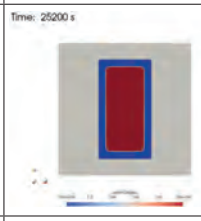
Discharging	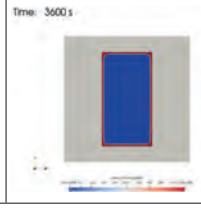	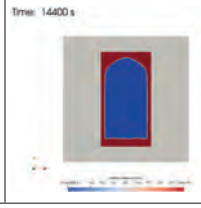	
Rollers			
Charging	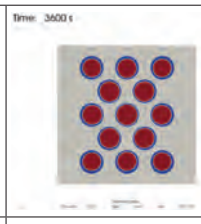	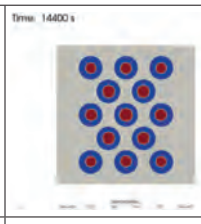	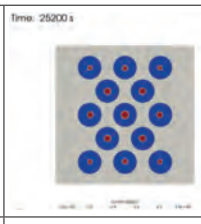
Discharging	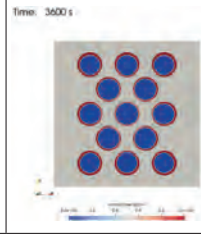	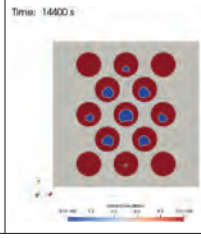	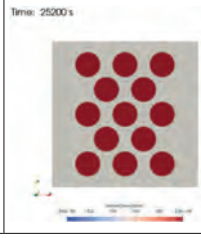
Grid			
Charging	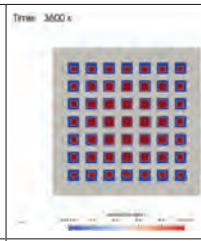	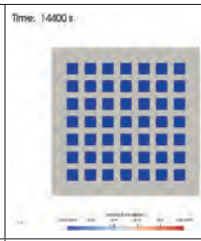	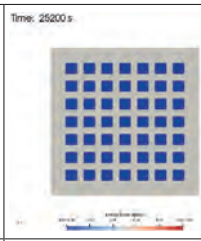
Discharging	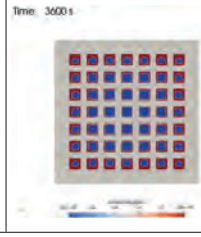	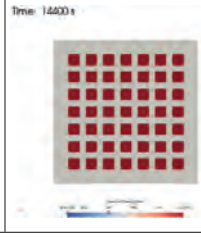	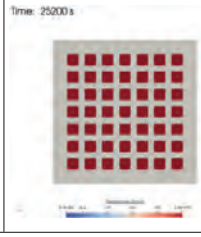

ratio of 43.60. It is worth considering further research and observing the dynamics of the process for geometries with an aspect ratio between 30 and 40, since for an aspect ratio of 43.60 there is an additional potential of 3 hours of charging and reducing the form factor would lengthen the discharge process.

Conclusions

In this paper, the geometry optimization of PCM energy storage was performed. Numerical calculations were conducted with the use of OpenFOAM software. To model solidification and melting of PCM, the enthalpy-porosity was applied. The results of the research demonstrate a high impact of the form factor on the dynamics of the phase change. The liquefying process was fully completed for three studied geometries. Entire process of solidification was achieved for two geometries. The most effective geometry obtained in this study is the geometry with horizontal ribs, because in the assumed time, the PCM for given conditions fully charges and discharges.

LITERATURE

[1] J. Yao, H. Xu, Y. Dai i M. Huang, „Performance analysis of solar assisted heat pump coupled with build-in PCM heat storage based on PV/T panel," *Solar Energy,* pp. 279-291, 2020, doi: 10.1016/j.solener.2020.01.002.

[2] F. Fornarelli, S. Camporeale, B. Fortunado, M. Torresi, P. Oresta, L. Magliocchetti, A. Miliozzi i G. Santo, „CFD analysis of melting process in a shell-and-tube latent heat storage for concentrated solar power plants," *Applied Energy,* pp. 711-722, 2016, doi: 10.1016/j.apenergy.2015.11.106 .

[3] T. Ma, Z. Li i J. Zhao, „Photovoltaic panel integrated with phase change materials (PV-PCM): technology overview and materials selection," *Renewable and Sustainable Energy Reviews,* tom 116, nr 109406, pp. 1-16, 2019, doi: 10.1016/j.rser.2019.109406.

[4] Y. Cui, J. Zhu, F. Zhang, Y. Shao i V. Xue, „Current status and future development of hybrid PV/T system with PCM module: 4E (energy, exergy, economic and environmental) assessments," *Renewable and Sustainable Energy Reviews,* tom 158, nr 112147, 2022, doi: 10.1016/j.rser.2022.112147 .

[5] „Rynek Mikroinstalacji Fotowoltaicznych Polska'19," Stowarzyszenie branży fotowoltaicznej Polska PV, 2020.

[6] V. Voller i C. Prakash, „A fixed grid numerical modelling methodology for convection-diffusion mushy region phase-change problems," *International Journal of Heat and Mass Transfer,* pp. 1709-1719, 1987, doi: 10.1016/0017-9310(87)90317-6.

[7] M. Rad, P. Kotas i C. Beckermann, „Rayleigh number criterion for formation of a-segregates in steel castings and ingots,," *Metallurgical and Materials Transactions A,* tom 44, pp. 4266-4281, 2013, doi: 10.1007/s11661-013-1761-4.

[8] P. Olafsson, R. Sandstrom i A. Karlsson, „Comparison of experimental, calculated and observed values for electrical and thermal conductivity of aluminium alloys.," *Journal of Materials Science,* tom 32, pp. 4383-4390, 1997, doi: 10.1023/A:1018680024876.

[9] „Pubchem Compound Summarry for CID 12398, Heptadecane," National Center for Biotechnology and Information. [Online]. [Data uzyskania dostępu: 7 11 2021].

[10] „Thermal Conductivity of Metals, Metallic Elements and Alloys," Engineering Toolbox, 2005. [Online]. Available: https://www.engineeringtoolbox.com/thermal-conductivity-metals-d_858.html. [Data uzyskania dostępu: 28 11 2021].

[11] „Heat of Fusion and Vaporization," gchem. [Online]. [Data uzyskania dostępu: 28 11 2021].

[12] Z. Jianrui, F. Yanhui, Y. Haibo, F. Daili, Z. Xinxin i W. Ge, „Thermal properties of C17H36/MCM-41 composite phase change materials," *Computational Materials Science,* tom 109, pp. 300-307, 2015, doi: 10.1016/j.commatsci.2015.07.033.

[13] „Specific Heat Capacity of Metals Table Chart," Engineering Reference and Online Tools, [Online]. Available: https://www.engineersedge.com/materials/specific_heat_capacity_of_metals_13259.htm. [Data uzyskania dostępu: 28 11 2021].

[14] „Weight & Density Of Aluminium 6061 G/Cm3, Lbs/In3, G/Ml, Lb/Ft3, G/Mm3, Cubic Inch," The World Material, [Online]. Available: https://www.theworldmaterial.com/weight-density-of-aluminum/. [Data uzyskania dostępu: 2021 11 28].

[15] A. Doolittle, „Studies in Newtonian Flow. II. The Dependence of the Viscosity of Liquids on Free-Space," *Journal of Applied Physics,* tom 22, nr 12, pp. 1471-1475, 14 Czerwiec 1951, doi: 10.1063/1.1699894. ■